International Journal of Gas Turbine, Propulsion and Power Systems
July 2024, Volume 15, Number 4

Low Reynolds Number Effects in Compressor Blade Design

A. Hergt, M. Pesch, S. Grund, J. Flamm

German Aerospace Center (DLR)
Institute of Propulsion Technology
Linder Höhe, 51147, Cologne, Germany

ABSTRACT

The trend for the engine design goes to smaller core engines to increase the bypass ratio and reduce the weight. With the decrease of core engine size, also the Reynolds Number decrease locally. This leads the focus within the design process of the axial compressor on the accuracy of the numerical models which are used for the simulation. Therefore, an experimental and numerical study was carried out to evaluate the state-of-the art design process for axial compressor bladings concerning the low Reynolds number effects within the flow. As study approach a linear cascade was used. Whereby the experiments were performed at the Transonic Cascade Wind Tunnel TGK of the DLR in Cologne and for the numerical simulations DLR in-house flow solver TRACE was conducted. The investigation was carried out at an inlet Mach number of 0.60 and a Reynolds number of 0.15 x 10^6. The comparison shows a significant discrepancy which is based on the current weakness of the turbulence and transition modeling at a RANS simulation regarding the viscosity effects at lower Reynolds numbers. Additional simulations were performed at a higher Reynolds number of 0.9 x 10^6 to substantiate this interpretation. Here, a good agreement with the equivalent measurement results at this Reynolds number is shown.

NOMENCLATURE

Latin

c	profile chord length
c_f	skin friction coefficient
h	blade span
de Haller	de Haller number = $\frac{v_2}{v_1}$
i	incidence angle = β_1-$\beta_{1,ADP}$
M	Mach number
p	pressure
Re	Reynolds number based on chord length
t	pitch
Tu	turbulence intensity
v	flow velocity
x, y, z	cartesian coordinates

Greek

β	flow angle with respect to cascade front
ε	cascade deflection angle = β_1-β_2
ω	total pressure loss coefficient = $\frac{p_{t,1}-p_{t,2}}{p_{t,1}-p_1}$
Ω	static pressure coefficient = $\frac{p_2-p_1}{p_{t,1}-p_1}$
ρ	density
τ_w	wall shear stress

Subscripts

0	reference state
1	inlet, inlet plane
2	exit, exit plane
s	stagger
t	total, stagnation value

Abbreviations

ASME	American Society of Mechanical Engineers
ADP	aerodynamic design point
AVDR	axial velocity density ratio = $\frac{\rho_2 \cdot v_2 sin\beta_2}{\rho_1 \cdot v_1 sin\beta_1}$
DLR	German Aerospace Center
DNS	direct numerical simulation
LES	large-eddy simulation
LRN	Low Reynolds number
MP 1	measurement plane 1 (inlet)
MP 2	measurement plane 2 (exit)
PS	pressure side
SS	suction side
RANS	Reynolds-averaged Navier-Stokes
TRACE	Turbomachinery Research Aerodynamic Computational Environment
TE	trailing edge

INTRODUCTION

Nowadays the design of the new engine generation also further trends to higher bypass ratios [7]. However, a further increase of the engine size is limited, since the outer diameter of a ducted fan engine is limited by their placement underneath the airplane wings as well as their weight increasing with the diameter. One way to meet this design challenge is to develop increasingly powerful small core engines.

However, this leads to new challenges as that tip leakage flow effects becomes more dominant [1]. A further key point here is that this further decreases the local Reynolds number in the compressor towards the range where the frictional forces become dominant over the inertial forces in the flow. Within a modern industrial design process optimization procedures as described by Voss et al. [17] are used and coupled with a flow solver. In the publications of Schreiber et al. [12, 13], Sonoda et al. [14, 15] and Hergt et al. [3, 6] it is visible that at low Reynolds number conditions the flow simulation with RANS is challenging and the accuracy of the

Manuscript Received on July 30, 2023
Review Completed on April 16, 2024

Fig.1 DLR Low Reynolds Number Cascade

Fig.2 DLR Transonic Cascade Wind Tunnel

Table 1 Cascade design parameter

Inlet Mach number	M_1	= 0.60
Inlet flow angle at ADP	β_1	= 133.0 deg
Reynolds number	Re	= 1.5 x 10^5
AVDR		= 1.03
Pitch to chord ratio	t/c	= 0.577
Turbulence intensity	Tu	= 0.50 %

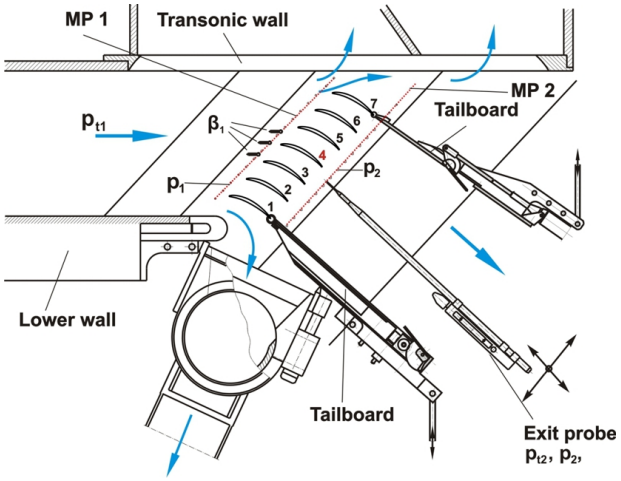

Fig.3 Cross section of the DLR Transonic Cascade wind tunnel

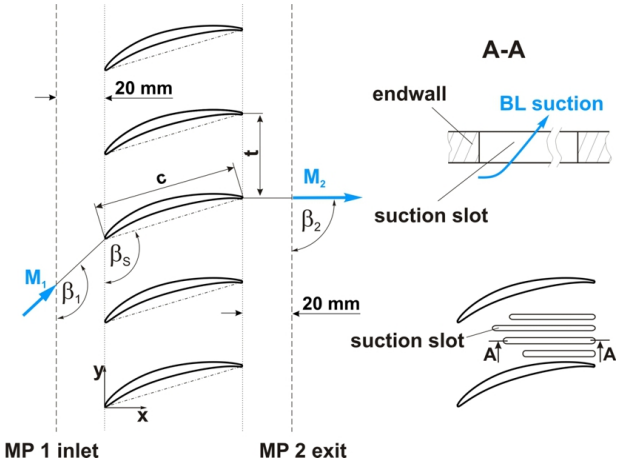

Fig.4 Cascade parameter, definition of measurement and analysis planes as well as boundary layer suction design

results is not ever sufficient ensured. For this reason, the possibility of using scale-resolved simulations such as LES up to DNS has been investigated for several years in order to improve the accuracy for special flow effects such as secondary flows [10], shocks [5, 8] or even low Reynolds numbers [9]. But at the moment, it is also clear that RANS methods are currently state-of-the-art in the design process, since the effort required to integrate scale-resolution methods is still very high. Therefore, this paper focuses on the question to what extent and how detailed the flow effects of a subsonic compressor profile at low Reynolds numbers are reproduced in RANS simulations based on a nowadays best practice approach.
In order to be able to answer this question, the paper shows the experimental results of a cascade measurement are compared with the results of the RANS simulation at a low Reynolds number of 0.15 x 10^6. The differences between the results are discussed in detail based on the occurring flow effects such as separation and boundary layer transition behavior. In addition, the experimental and numerical results at a significantly higher Reynolds number of 0.9 x 10^6 are also used for comparison. This allows the differences at the lower Reynolds number to be highlighted even more clearly and should show how accurate the simulation results of the RANS method are with these boundary conditions. It also enables to detect any ”non” Reynolds number effects that may occur. Such effects could be a deviation in the general operating behavior of the cascade at both Reynolds number conditions.

INVESTIGATION SETUP

As already mentioned a linear compressor cascade is used for the study. Figure 1 shows the experimental DLR LRN (Low-Reynolds-Number) cascade [6] which consists of 6 blades. An overview of the general design parameter of this cascade is given in Tab. 1. This cascade was originally developed for the application of riblets [3] and therefore the datum cascade is designed for low Reynolds number conditions at Re = 1.5 x 10^5. Based on this cascade, a setup for the numerical simulations and experimental investigation in this study is now derived. Since this is a profile-only study, measurements will be made exclusively in the mid-section of the cascade. And also the numerical simulation will be done on a quasi-3D (Q-3D) mesh.

Experimental Setup

The experiments were carried out in the Transonic Cascade Wind Tunnel [4, 11, 16] at DLR in Cologne as shown in Fig. 2. This wind tunnel is a closed loop facility and enables a continuously testing. The test section is equipped with a variable nozzle and an upper

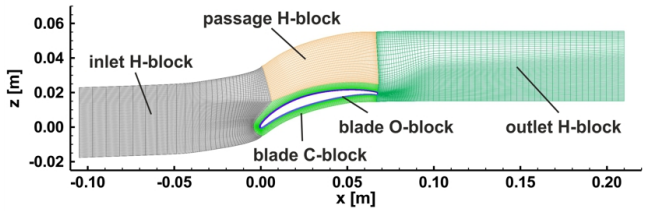

Fig.5 Structured Mesh with an O-C-H topology and 6.8 x 10^5 nodes

Table 2 Solver and convergence settings for TRACE calculations

	Criterion	Settings
Simulation mode	steady	
Spatial scheme		Fromm Scheme
	accuracy	2nd order
	limiter	VanAlbadaSqr
Time scheme	solution method	PredictorCorrector
Turbulence model	SST k-ω	
Transitions model	γ-Re-θ	
Gas model	ideal	
Convergence control	mass flow at $\Delta = 0.01$	

transonic wall in order to reduce shock reflection. The variable test section height is necessary to adjust the test section on the specific cascades. Suction capacities at the endwalls are used to adjust the operating points of the cascade.
Figure 3 shows the test section with the arrangement of the blades as well as the position of the measurement planes MP 1 in front and MP 2 behind the cascade. Furthermore, the position of the three inflow angle probes and the wake probe is shown. Conventional static pressure measurement was used at inlet measurement plane (MP 1) and exit measurement plane (MP 2) in addition to the measurement of the total pressure in the settling chamber as well as in the wake at MP 2 by means of a 3-hole probe. This probe provides also the outflow angle of the cascade and is used to determine the total pressure loss. On the suction and pressure side surface at mid-span of blade no. 4 and 5 the profile Mach number distribution of the cascade was measured by static pressure taps. The operating point of the cascade is clearly determined by this Mach number distribution and by the inflow and outflow conditions as well as the AVDR.
In Addition to that, the cascade parameter as well as the design of the boundary layer suction slots within the cascade passages are shown in Fig. 4. This suction system was necessary during the test in order to adjust the AVDR of 1.03.

Numerical Setup

The 3D RANS flow solver TRACE is used to perform the simulations. The name TRACE stands for "Turbomachinery Research Aerodynamic Computational Environment". This is the in-house development solver of the Institute of Propulsion Technology (DLR). Table 2 shows an overview of the best practice setup which was used for the investigation.
The meshing of the geometries was performed with the software PyMesh. This software is also an in-house development and specially customized for turbomachinery application. It is a structured multi-block mesher, whereby an O-C-H multi-block mesh consisting of seven blocks is created on the S1 plane as shown in Fig. 5. Since a Q-3D study supposed to performed, the extent of the mesh in the S2 plane is 7 nodes which corresponds to 5 mm at the inlet of the mesh. The inlet length in front of the leading edge is 1.5

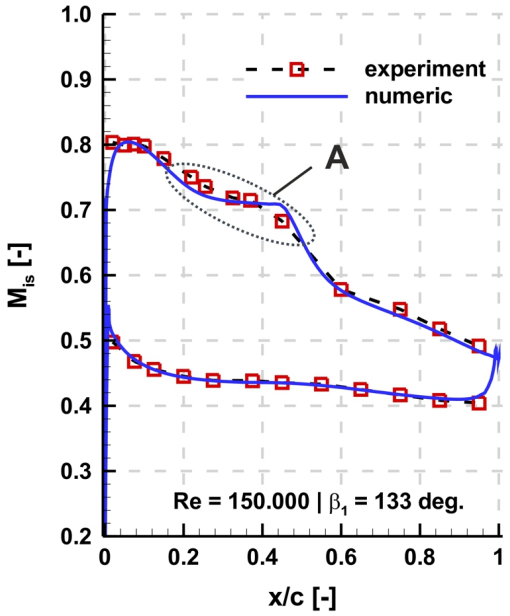

Fig.6 Experimental and numerical isentropic Mach number distribution at Re = 1.5 x 10^5 and an inlet angle of 133 deg. (ADP)

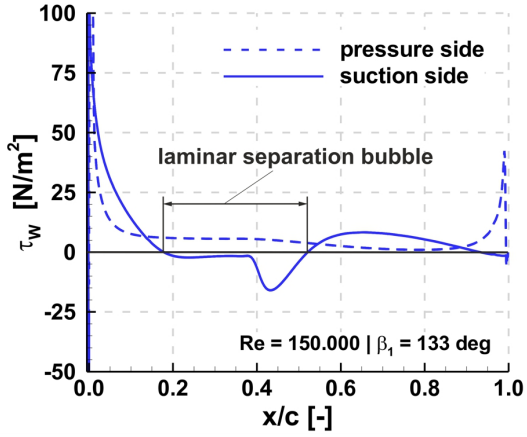

Fig.7 Numerical wall shear stress distribution at Re = 1.5 x 10^5 and an inlet angle of 133 deg. (ADP)

times and the outlet length behind the trailing edge 2 times the profile chord length c. Furthermore, the AVDR of 1.03 is considered by using a linear contraction from blade leading to trailing edge in the S2 plane.
The used mesh was derived from a mesh study which was conducted at the beginning of the investigation. Therefore, three different sized meshes were build in order to find a compromise between minimum needed mesh size for a sufficient accuracy. In order to quantify the discretization error and to assess the mesh quality, the grid convergence index (GCI) method by ASME was used. Based on this procedure, only the fine mesh with 6.8 x 10^5 nodes fulfilled the requirements and was finally used for the investigation.

RESULTS AND DISCUSSION

Behavior at the Aerodynamic Design Point

The first step of the study focuses on the aerodynamic design point of the cascade at an inflow angle of 133 deg. and a Reynolds number of Re = 1.5 x 10^5. Figure 6 shows the experimental and numerical isentropic Mach number distribution at this operating

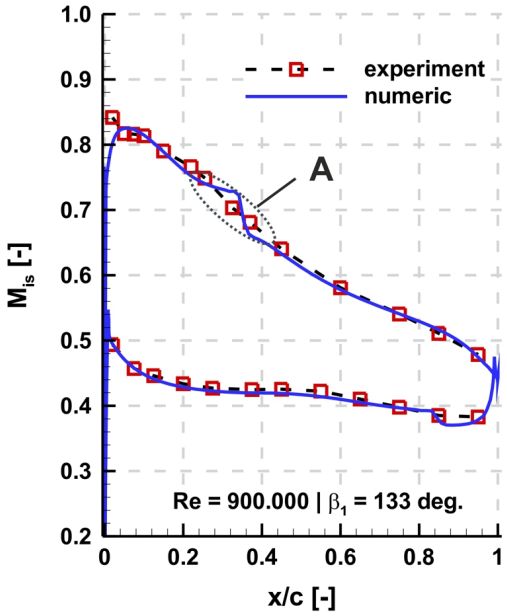

Fig.8 Experimental and numerical isentropic Mach number distribution at Re = 9.0 x 10^5 and an inlet angle of 133 deg. (ADP)

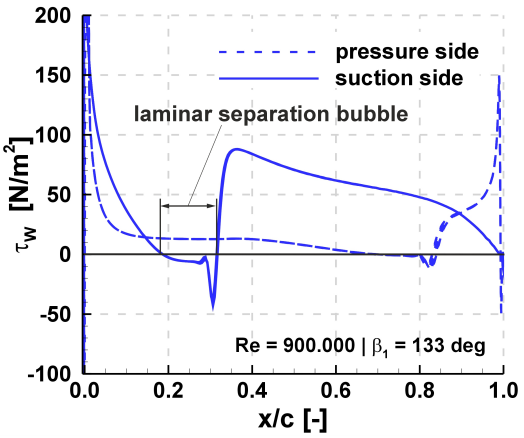

Fig.9 Numerical wall shear stress distribution at Re = 9.0 x 10^5 and an inlet angle of 133 deg. (ADP)

point. Basically, the distributions seems to match very well. In particular, it should be noted that the size of the symbols of the experimental results in the diagram represents the measurement uncertainty. Against this background, the pressure side distribution shows an outstanding agreement. Nevertheless, in the area of the suction-side distribution labeled with A, a discrepancy is noticeable. This deviation occurs in the region of the laminar separation bubble. Therefore, it can be assumed that the appearance of the separation bubble differs between the experiments and the numerical simulations. A clear statement about the influence of this deviation is not directly possible from the Mach number distribution.

Therefore, a closer look at the behavior of the separation bubble is necessary. During the experiments, injection tests were carried out in which ink was injected through the suction side pressure hole number 7. This ink gathered inside the bubble and allowed the determination bubble extension of about 20 percent of the chord length. The determination of the extent of the laminar separation bubble in the numerical results is possible by means of the wall

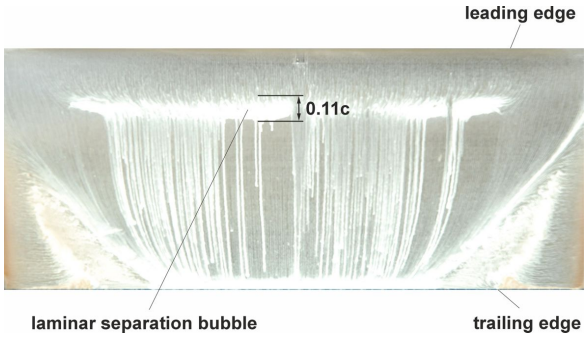

Fig.10 Oil flow visualization on the blade suction side at Re = 9.0 x 10^5 and an inlet angle of 133 deg. (ADP)

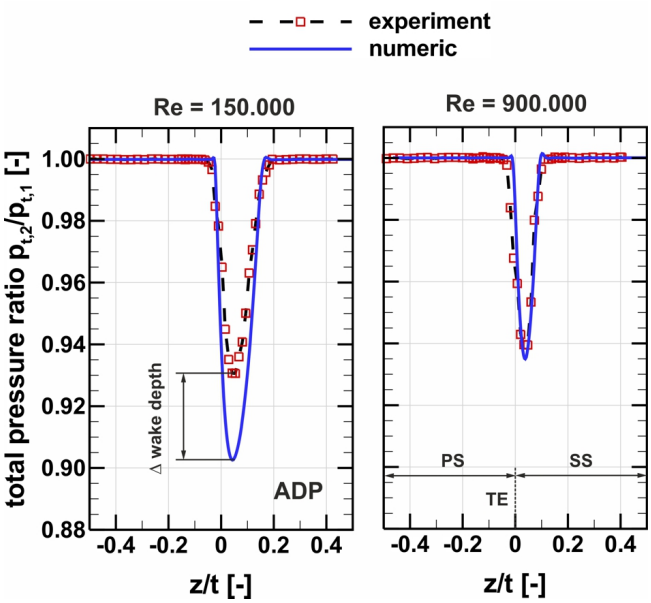

Fig.11 Experimental and numerical total pressure ratio at MP 2 and both Reynolds numbers and an inlet angle of 133 deg. (ADP)

Table 3 Total pressure loss coefficients at ADP

Re:	**1.5 x 10^5**	**9.0 x 10^5**
Exp.	0.033	0.019
Num.	0.043	0.016
Difference	+ 29%	- 14 %

shear stress distribution on the blade surface, as shown in Fig. 7. Here it can be seen that the suction side distribution of the wall shear stress has a negative value from x/c = 0.18 to 0.51. This corresponds to an extension of the laminar separation bubble of about 33 percent of the chord length which is 65 percent larger compared to the experimental result. And despite of only a slight differences in the isentropic Mach number distribution, there is a significant change in the flow pattern with respect to the suction side transition at this low Reynolds number.

It is expected that this will have a significant effect on the overall performance of the cascade. But before this is considered in more detail hereafter, a comparison with the results at a higher Reynolds number of 9.0 x 10^5 will be made. Figure 8 shows the isentropic

Mach number distribution at this Reynolds number and it becomes evident that the distributions match extremely good. The region of the suction side laminar separation bubble marked with A shows only very slight deviations between the experimental and numerical results. These first results in ADP suggest that the simulation results at low Mach numbers have a significant difference to the experimental results, whereas at higher Reynolds numbers the agreement is considerably better.

This assessment is also supported by Fig 9. Here, the suction side distribution of the wall shear stress on both blade side is shown for the higher Reynolds number. The extension of the laminar separation bubble is marked and amounts to 12 percent of the chord length. This means that the separation bubble is 63 percent smaller than for the low Reynolds number case. For the flow case with a higher Reynolds number, oil flow visualizations were produced as shown in Fig 10. In this figure the laminar separation bubble is visible and its extension is 11 percent of chord length. This means that the numerical simulation predicts the size of the laminar separation bubble very accurately at high Reynolds numbers

In order to better understand what the significant difference in transition behavior at small Reynolds numbers means, the loss behavior is considered in the next step. For this purpose, the experimental and numerical wake of the total pressure ratio at both Reynolds numbers are shown in Fig. 11. It can be seen that the wake is significantly deeper for the small Reynolds number in the simulation. Whereas the wakes at the higher Reynolds number agree very well. In Tab. 3, the averaged total pressure loss coefficients are plotted and it can be seen that for the small Reynolds number, the difference of 29 percent is very high. In addition, a fundamental behavior becomes clear here. At the low Reynolds numbers, the losses are overestimated in the numerical simulation, whereas at the high Reynolds numbers, the losses are underestimated.

Operating Range Behavior

This statement only looks at the aerodynamic design point. Beyond that, the behavior at the operating range limits is essential for the evaluation of the compressor cascade performance. Figure 12 shows the wakes near the choke point of the cascade with an incidence angle of -5 deg. At the high Reynolds number, there is very good agreement between the wakes, and the differences in loss coefficients between experiment and numerics is only - 7 percent. A similar tendency can be observed for the low Reynolds number, where the difference in the loss coefficient decreases to 18 percent. However, this reduction in the difference at the low Reynolds number results from two effects, which come together and are superimposed. If only the difference in the depth of the wake is considered, it is clear that this is larger at - 5 deg. incidence than in the ADP. On the other hand, the wake width is slightly underestimated in the simulation compared to the experiment, which results in the overall reduced difference in the total pressure loss coefficient.

In Fig. 13 the total pressure loss characteristics are shown and from this it is possible to assess the entire loss behavior over the operating range of the cascade. The part of the characteristic from the ADP towards close to the choke boundary has already been described. Starting from the ADP in the direction of a positive incidence angle, representing an increase in the aerodynamic load on the cascade, the picture changes at the low Reynolds number. With the Reynolds number of 9.0 x 10^5 and an incidence i = + 3 deg. the experimental and numerical losses are almost unchanged and the difference between them is also nearly constant. Whereas for the Reynolds number of 1.5 x 10^5, the numerical losses increase significantly while the experimental ones increase only minimally. This behaviour is marked with A in the figure and leads to the fact that the discrepancy between the experimental and numerical results increases further. The difference in the total pressure loss coefficients is already 39 percent in this case and this means that the tendency

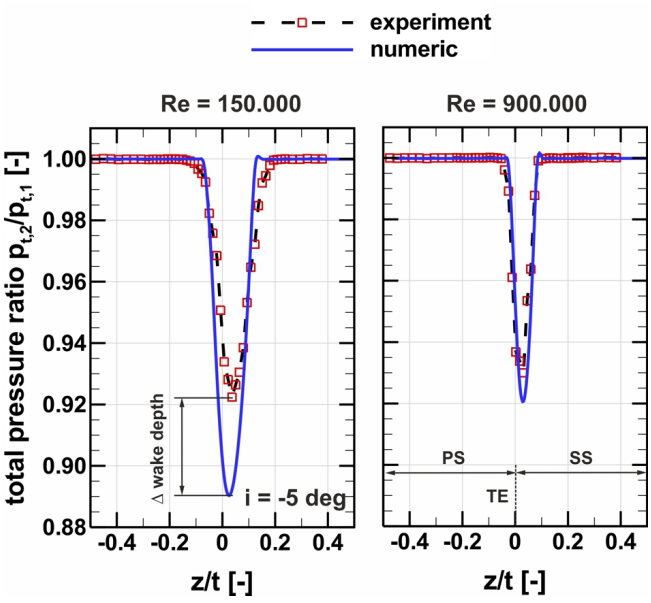

Fig.12 Experimental and numerical total pressure ratio at MP 2 and both Reynolds numbers and an inlet angle of 128 deg. (i = -5 deg)

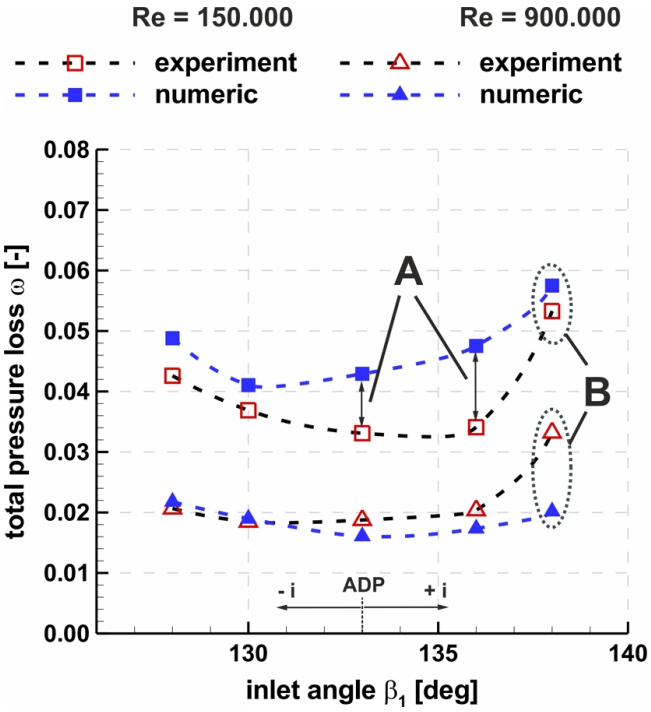

Fig.13 Experimental and numerical total pressure loss characteristics at both Reynolds numbers

to overestimate the losses by the numerics becomes even greater. When approaching the separation boundary of the cascade at an inflow angle of 138 deg. there is a change in the loss behavior for the two Reynolds numbers which is marked with B in Fig. 13. The experimental losses at the high Reynolds number increase significantly close to the separation boundary, whereas the numerical losses increase only to a small extent. This leads to an even more significant underestimation of the losses by the numerics. A look at the wakes in Fig. 14 gives an idea of what is going on at the high Reynolds number. While in the simulation a proper flow around the cascade profiles is still noticeable on the basis of the wake, the wake of the experiment shows due to higher losses (marked with B) that

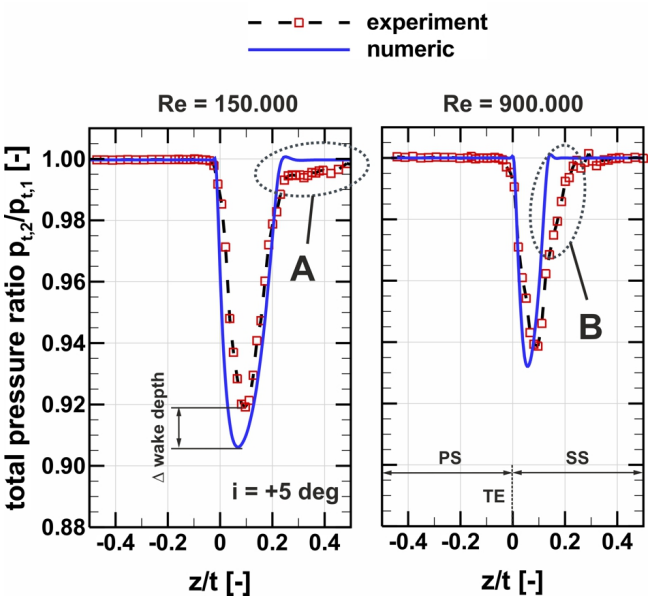

Fig.14 Experimental and numerical total pressure ratio at MP 2 at both Reynolds numbers and an inlet angle of 138 deg. (i = +5 deg)

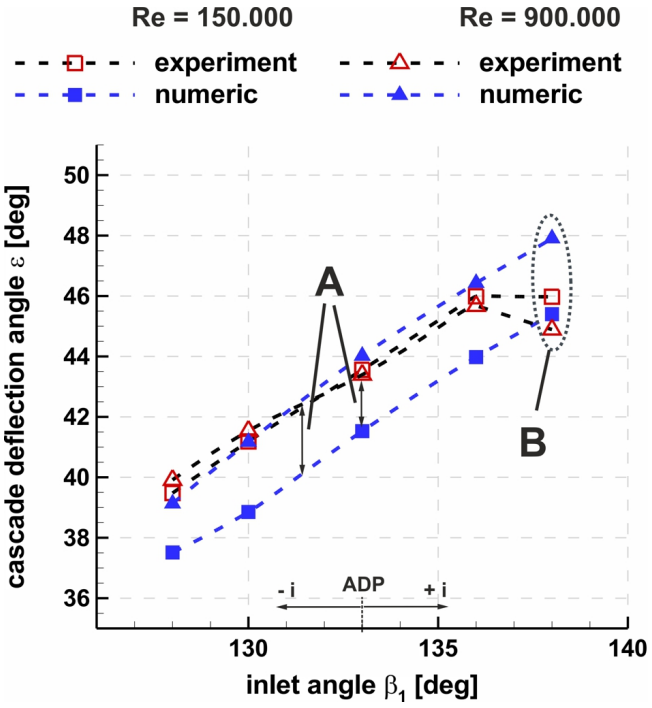

Fig.15 Experimental and numerical cascade deflection characteristics at both Reynolds numbers

here a part of the flow is separated on the suction side. The experimental separation boundary of the cascade is already reached and and is not adequately predicted by numerics.

At the low Reynolds number, the behavior is basically similar. Figure 14 also clearly shows that flow separation already occurs in the suction side of the wake (marked with A). Also in this case, the separation boundary of the cascade is reached in the experiment. However, this results in a reduction of the discrepancy between the numerically determined total pressure loss and the experimentally measured one. But also in this case it becomes clear that the experimental boundary of the working range of the cascade could not be predicted by the numeric.

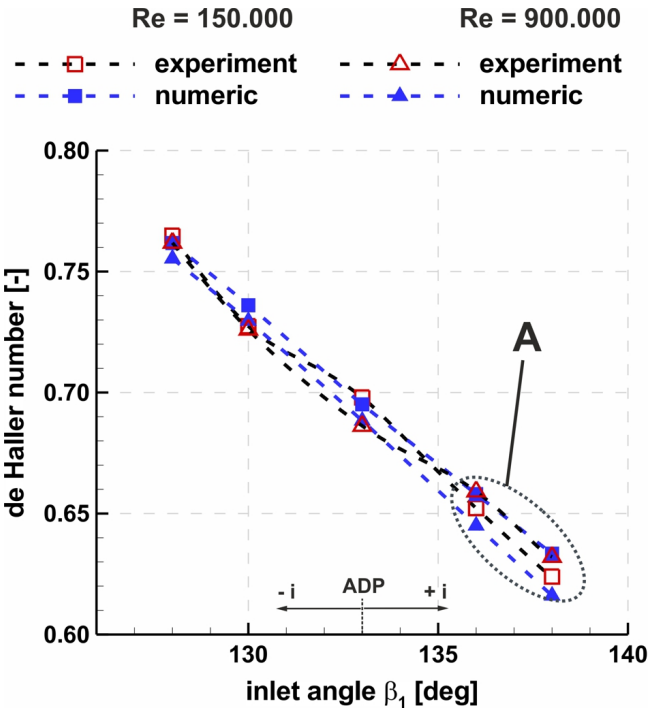

Fig.16 Experimental and numerical de Haller number characteristics at both Reynolds numbers

In the following, the influence of these discrepancies between the experimental and numerical loss results on the further cascade performance parameters as deflection, deceleration and pressure rise will be evaluated. Figure 15 shows the cascade deflection characteristics for both Reynolds numbers. In contrast to the losses, it is evident here that the experiments show a Reynolds number-independent behavior. The plots agree well with each other. The numerical results for the cascade deflection at high Reynolds numbers also agrees very well with the experiments. However, considerable deviations can be seen at the separation boundary at an incidence angle of + 5 deg wich is marked with B in Fig. 15. These can be clearly traced back to the already described fact that the working range boundary could not be predicted with sufficient accuracy by numerical methods. Furthermore, the results also show that the cascade deflection is consistently underestimated by the numerics at the low Reynolds number. This behaviour is marked with A in the figure and illustrates that in this case the deflection is 2 deg. too low over the working range. It can be assumed that this behavior at the low Reynolds number results from the significantly larger laminar separation bubble and the resulting thicker downstream boundary layer. The flow cannot adequately follow the deflection through the profiles anymore.

The characteristic of the de Haller number shown in Fig. 16 is a measure of the deceleration due to the cascade. Usually, in the literature, it is considered that de Haller numbers smaller than 0.7 correspond to a very high aerodynamic load. This means that the DLR LRN cascade is very highly loaded, since the de Haller number is already just below 0.7 in the ADP. Nevertheless, the cascade shows a deceleration on a comparative level in all cases. The significant differences in loss behavior are not reflected here. A marginal widening of the curve occurs only in the operating points with positive incidence, which are marked with A.

The effective rise in static pressure over a compressor cascade depends not only on the deflection and the deceleration, but also to a large extent on the loss behavior. Therefore the following picture appears in Fig 17. In ADP and at negative incidence angles, the static pressure coefficients at the high Reynolds number agree

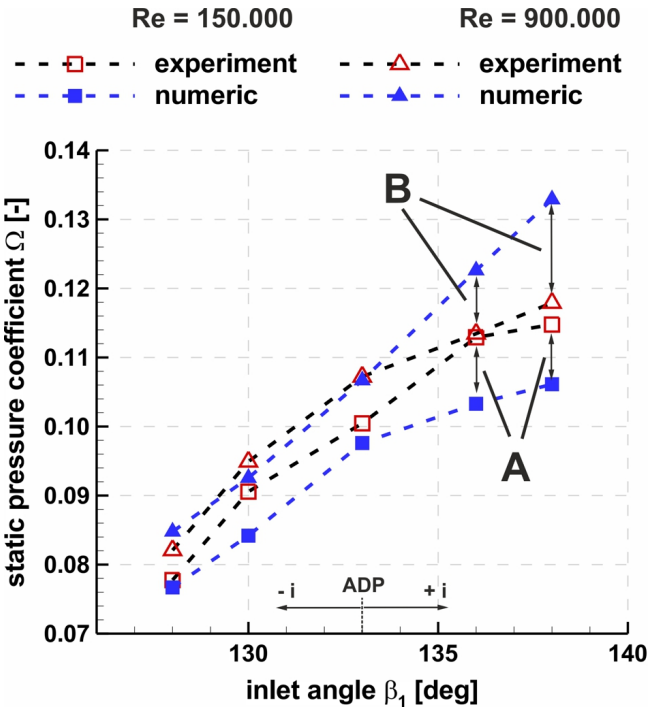

Fig.17 Experimental and numerical static pressure coefficient characteristics at both Reynolds numbers

very well between experiment and numerics. Results differ considerably only in the area of positive incidence. Despite a comparable deceleration and deflection, the cascade can no longer realize the pressure increase to the same extent as predicted by the numerics due to the increasing losses. The opposite behavior is seen at the low Reynolds number. Due to the considerable overestimation of the losses, the static pressure increase is underestimated in the numerical simulations over the working range.
Finally, it must be noted that there is still a significant discrepancy between experimental and numerical results at small Reynolds numbers.

Recommendation on the Numerical Approach

The presented results show very clearly that there is still a recognizable discrepancy between the numerical simulation and the experiments. Furthermore, it becomes clear that the deviation strongly depends on the Reynolds number and the aerodynamic load. The deviations increase with decreasing Reynolds number as well as increasing aerodynamic load. Both the transition behavior and the separation behavior were detected as crucial aerodynamic mechanisms. In the RANS simulations, the used SST k-ω turbulence model and γ-Re-θ transition model can be clearly identified as the relevant methods, as these determine the separation behavior and the transition. The best practice approach was specifically chosen in the study, as the aim was to reflect the current status of the compressor design process. Nevertheless, an initial improvement of the numerical results could be possible by using a different turbulence model. Since at low Reynolds numbers the viscous effects in the flow dominate over the inertial effects and therefore more separation-related flow states (transition bubble, trailing edge separation) occur, the use of a turbulence model that better reflects anisentropic Reynolds stress behavior could improve the flow prediction. One possibility would be the Hellsten EARSM k-ω model [2]. In this model, the assumption of eddy viscosity is replaced by a more general relationship for the Reynolds stress anisotropy. A more advanced approach is the use of scale-resolving methods such as LES. Their use would be particularly effective with low Reynolds numbers, as in this case the calculation times can be significantly reduced compared to applications with high Reynolds numbers. Compared to RANS simulations, however, the resources required are currently still too high to use LES in an industrial optimization-based design process. Thus, it is foreseeable that an ever-increasing demand for high-precision numerical simulations can only be met by using scale-resolving methods.

CONCLUDING REMARKS

An extensive experimental and numerical study of the low Reynolds number effects in axial compressor blade design was performed. The objective was to compare the experimental and numerical results, based on a state-of-the-art RANS simulation approach, to assess how accurately the low Reynolds number flow can be estimated.
The results shows that the RANS simulation does not full fill the design aim at low Reynolds number flow, because there are significant deviations as exemplary shown by wake measurements. Primarily, this is reflected in the loss behavior of the cascade. The numerical results overestimate the losses over the entire operating range. Furthermore, it was shown that an adequate prediction of the operating boundary at positive incidence was not possible. In addition, the simulations showed a consequentially reduced deflection by 2 deg. over the working range. From the considerable differences in the losses and the cascade deflection, there is also a significant deviation with respect to the static pressure rise.
In conclusion, the main result of the study is that the best practice RANS approach applied for the simulation shows a considerable lack of accuracy in the prediction of compressor flows at low Reynolds number conditions. To further improve the quality of the simulations, it is recommended to focus on the selection of the turbulence model for such cases. Further improvement of the models is currently being targeted. However, in the future the research should more and more focused on the further development of scale-resolving methods and processes. If the prediction accuracy has to be significantly improved further, their application in compressor design is crucial and particularly foreseeable for applications with low Reynolds numbers.

References

[1] R. A. Berdanier and N. L. Key, *The Effects of Tip Leakage Flow on the Performance of Multistage Compressors Used in Small Core Engine Applications*, ASME Journal of Engineering for Gas Turbines and Power, 138(5) (2016).

[2] A. Hellsten, *New advanced k-w tuburlence model for high-lift aerodynamics*, AIAA Journal, 43(9) (2005), p. 18571869.

[3] A. Hergt, W. Hage, S. Grund, W. Steinert, M. Terhorst, F. Schongen, and Y. Wilke, *Riblet application in compressors: Toward efficient blade design*, ASME Journal of Turbomachinery, 137 (2015), p. 111006.

[4] A. Hergt, J. Klinner, S. Grund, C. Willert, W. Steinert, and M. Beversdorff, *On the Importanceof Transition Control at Transonic Compressor Blades*, ASME Journal of Turbomachinery, 143 (2021), p. 031007.

[5] A. Hergt, B. Klose, J. Klinner, M. Bergmann, E. J. M. Lopez, S. Grund, and C. Morsbach, *On the Shock Boundary Layer Interaction in Transonic Compressor Blading*, in ASME Turbo Expo, GT-2023-103218, June 26-30, Boston, MA, USA, 2023.

[6] A. Hergt, W. Steinert, and S. Grund, *Design and Experimental Investigation of a Compressor Cascade for Low Reynolds Number Conditions*, no. ISABE-2013-1104 in 21st ISABE Conference, Busan, Korea, 9-13 September 2013.

[7] B. Kaplan, E. Nicke, and C. Voss, *Design of a highly efficient low-noise fan for ultra-high-bypass engines*, no. GT2006-90363 in ASME Turbo Expo, Barcelona, Spain, June 2006, ASME.

[8] B. F. Klose, C. Morsbach, M. Bergmann, A. Hergt, J. Klinner, S. Grund, and E. Kügeler, *A Numerical Test Rig for Turbomachinery Flows Based on Large Eddy Simulations with a High-Order Discountinuous Galerkin Scheme - Part 2: Shock-Capturing and Transionic Flows*, in ASME Turbo Expo, GT-2023-101374, June 26-30, Boston, MA, USA, 2023.

[9] Q. Liu, W. Ager, C. Hall, and A. P. Wheeler, *Low Reynolds Number Effects on the Separation and Wake of a Compressor Blade*, ASME Journal of Turbomachinery, 144(10) (2022).

[10] C. Morsbach, M. bergmann, A. Tosun, B. F. Klose, P. Bechlars, and E. Kügeler, *A Numerical Test Rig for Turbomachinery Flows Based on Large Eddy Simulations with a High-Order Discountinuous Galerkin Scheme - Part 3: Secondary Flow Effects*, in ASME Turbo Expo, GT-2023-101374, June 26-30, Boston, MA, USA, 2023.

[11] H. A. Schreiber, H. Starken, and W. Steinert, *Transonic and Supersonic Cascades*, AGARDOgraph - Advanced Methods for Cascade Testing, AGARD AG 328 (1993), pp. 35–59.

[12] H. A. Schreiber, W. Steinert, and B. Kuesters, *Effects of Reynolds Numbers and Free-Stream Turbulence on Boundary Layer Transition in a Compressor Cascade*, ASME Journal of Turbomachinery, 124 (2002), pp. 1–9.

[13] H. A. Schreiber, W. Steinert, T. Sonoda, and T. Arima, *Advanced High Turning Compressor Airfoils for Low Reynolds Number Condition-Part II: Experimetal and Numerical Analysis*, ASME Journal of Turbomachinery, 126 (2004), pp. 482–492.

[14] T. Sonoda and H. A. Schreiber, *Aerodynamic Characteristics of Supercritical Outlet Guide Vanes at Low Reynolds Number Conditions*, ASME Journal of Turbomachinery, 129 (2007), pp. 694–704.

[15] T. Sonoda, Y. Yamaguchi, T. Arima, M. Olhofer, B. Sendhoff, and H. A. Schreiber, *Advanced High Turning Compressor Airfoils for Low Reynolds Number Condition-Part I: Design and Optimization*, ASME Journal of Turbomachinery, 126 (2004), pp. 350–359.

[16] W. Steinert, R. Fuchs, and H. Starken, *Inlet Flow Angle Determination of Transonic Compressor Cascade*, ASME Journal of Turbomachinery, 114 (1992), pp. 487–493.

[17] C. Voss, M. Aulich, and B. Kaplan, *Automated Multiobjective Optimisation in Axial Compressor Blade Design*, no. GT2006-90420 in ASME Turbo Expo, Barcelona, Spain, 08-11 May 2006.